Selgin Al*, Nihat Arikan and Ahmet Iyigör

Investigations of Structural, Elastic, Electronic and Thermodynamic Properties of X_2TiAl Alloys: A Computational Study

https://doi.org/10.1515/zna-2018-0207
Received April 19, 2018; accepted June 1, 2018; previously published online June 22, 2018

Abstract: First-principle calculations have been adopted in order to reveal and deeply understand the structural, electronic, elastic, thermodynamic, and vibrational properties of full-Heusler X_2TiAl (X = Au, Ru, and Zr) alloys in the $L2_1$ phase. The fundamental physical properties such as bulk modulus, its pressure derivative, anisotropy factor, shear modulus, Poisson's ratio, Cauchy pressure, elastic constants, heat capacity, thermal expansion coefficient, and Young's modulus are obtained and compared with the literature. Debye temperature and Grüneisen parameter are also evaluated over the temperature range of 0–1500 K. Electronic band structures and their partial density of states and phonon dispersion curves are presented for all alloys and used to interpret the electronic and mechanical properties and stabilities of alloys in the $L2_1$ phase.

Keywords: DFT; Elastic Constant; Electronic Structure; First Principle; Phonon.

PACS Number: 71.20.Lp; 74.25.Jb; 74.25.Ld; 74.25.Kc.

1 Introduction

Since the discovery of Heusler alloys in 1903, they have been taking increasing attention by the researchers because of their unusual thermal, electrical, magnetic, and transport properties. For instance, ferromagnetic alloys can be produced from non-ferromagnetic materials [1]. These ternary alloys are in the form of X_2YZ where X and Y are generally transition metals and Z is a main group metal with *sp* electrons. The first studied Heusler alloys were crystallised in $L2_1$ phase, consisting of four fcc sub-lattice. Then, the $C1_b$ phase was discovered where it is possible to leave one of the four fcc sub-lattice. Thus, they are usually called half or semi Heusler alloys or just Heuslers, while $L2_1$ phase alloys are known as full Heusler alloys. These alloys have wide physical properties such as half-metallicity [2–5], thermodynamic [6, 7], shape memory effect [8, 9], heavy fermion behaviour [10–12], magnetic ordering [13, 14], and superconductivity [15]. Therefore, they are still of great interest for technological applications. However, it is not applicable to synthesise all the possible alloys and investigate their properties experimentally. Hence, a much efficient, reliable, and faster tool, first-principle calculation method, is adopted by the researchers that can provide accurate and substantial information about these materials and allow one to go through numerous intended materials without wasting much time and resources. For example, by calculating elastic constants of an alloy, various information about atomic bondings, stability, and mechanical and thermodynamic properties of the material can be extracted.

Because of the mentioned reasons above, Au_2TiAl, Ru_2TiAl, and Zr_2TiAl alloys have drawn our attention owing to their lack of detailed properties in the literature to the best of our knowledge. The structural properties of Au_2TiAl alloy were experimentally studied by Marazza et al. [16] by means of X-ray diffraction. Their data suggested a CsCl structure for this alloy. A few thermodynamic parameters were also studied in literature; for instance, Watson et al. [17] calculated the heat of formation for many ternary transition metal aluminide alloys, including Au_2TiAl and Ru_2TiAl. Ying and Nash [18] studied a series of Ru-based Heusler compositions. They measured standard enthalpy of formation using high-temperature direct reaction calorimetry. Yang et al. [19] investigated phase properties of Zr_2TiAl alloy by electron probe micro analyser and X-ray diffraction. Sornadurai et al. [20, 21] studied the crystal structure, microstructure, and mechanical and phase properties of the Zr_2TiAl alloy by using scanning electron microscopy and energy dispersive X-ray analysis. They indicated that Zr_2TiAl has three phases;

***Corresponding author: Selgin Al,** Department of Physics, Faculty of Arts and Sciences, Ahi Evran University, Kırşehir, Turkey, Tel.: 00903862803110, E-mail: selgin.al@ahievran.edu.tr
Nihat Arikan: Department of Mathematics and Science, Education Faculty, Ahi Evran University, Kırşehir, Turkey
Ahmet Iyigör: Ahi Evran University, Central Research Lab, 40100 Kırşehir, Turkey

however, the major phase was the stoichiometric Zr_2TiAl alloy. The electronic, magnetic, and mechanical properties of Zr_2TiAl were investigated using full potential linear augmented plane wave method by Reddy and Kanchana [22]. Their result indicated a ductile nature for this alloy. A few existing experimental and theoretical studies do not present a full systematic information about these alloys and will not be enough to design experiments to upgrade these alloys' related properties. Thus, in this work, their structural, electronic, mechanical, and thermodynamic properties are systematically investigated by means of first-principle calculations for the Heusler alloys X_2TiAl (X = Au, Ru, and Zr). A series of physical parameters, such as lattice constant, bulk modulus, bulk modulus pressure derivative, elastic constants, Cauchy pressure, specific heat capacity, thermal expansion coefficient, Debye temperature, Grüneisen parameter, and anisotropy factory, are presented. Band structures, density of states, and phonon dispersion curves are also evaluated and presented in this study for the first time.

2 Method of Computation

All the calculations based on ab initio density functional theory [23, 24] was carried out by using the Quantum-Espresso software package [25]. Perdew-Burke-Ernzerhof generalised gradient approximation (PBE-GGA) was used for the exchange correlation potential [26]. The electronic wave functions were expanded in plane wave basis to set up a kinetic energy cutoff to 40 Ry, while the cut off energy for the electronic charge density was set to 400 Ry. A $10 \times 10 \times 10$ k-point mesh was utilised to sample the Brillouin zone. A Methfessel-Paxton [27] smearing parameter with a width of $\sigma = 0.02$ Ry was applied for the integration up to the Fermi surface. The lattice dynamic calculations were done within the framework of the density functional perturbation theory [28, 29]. The phonon frequencies were calculated on a $4 \times 4 \times 4$ q-point mesh in order to obtain eight dynamic matrices. Fourier deconvolution was applied to this mesh to evaluate these dynamical matrices at arbitrary wave vectors. Specific heats at a constant volume versus temperature were computed using the quasi harmonic approximation [30].

A cubic crystal is generally represented by three independent elastic constants (namely, C_{11}, C_{12}, and C_{44}). The simple way of obtaining these constants is to calculate them from the energy difference between an unstrained medium and a distorted medium in a constant volume. Bulk modulus B, C_{44}, and shear modulus, $C' = (C_{11} - C_{12})/2$, were computed using hydrostatic pressure, $e = (\delta, \delta, \delta, 0, 0, 0)$, tri-axial shear strain, $e = (0, 0, 0, \delta, \delta, \delta)$, and volume-conserving orthorhombic strain, $e = (\delta, \delta, (1+\delta)^{-2} - 1, 0, 0, 0)$. The strain ($\delta$) was taken as 0.02 for 21 sets of calculations $\left(\frac{\Delta E}{V}\right)$. Then, the bulk modulus was obtained as follows:

$$\frac{\Delta E}{V} = \frac{9}{2} B \delta^2 \tag{1}$$

where V corresponds to the lattice cell volume before strain, ΔE expresses energy change due to strain and is represented by a vector; $e = (e_1, e_2, e_3, e_4, e_5, e_6)$. The relationship between energy change and shear modules, C', can be given as follows:

$$\frac{\Delta E}{V} = 6C'\delta^2 + 0\delta^3 \tag{2}$$

$C_{11} = (3B + 4C')/3$ and $C_{12} = (3B - 2C')/3$ are obtained from (2). C_{44} is computed from the following equation:

$$\frac{\Delta E}{V} = \frac{3}{2} C_{44} \delta^2 \tag{3}$$

The shear modulus (G; resistance of the material towards elastic deformation) is the ratio of shear stress to shear strain and given by

$$G = \frac{G_v + G_R}{2} \tag{4}$$

where G_v is Voigt's shear modulus and G_R is Reuss's shear modulus. G_v and G_R correspond to the upper and lower bounds of G, respectively, and are expressed as follows:

$$G_v = \frac{C_{11} - C_{12} + 3C_{44}}{5} \tag{5}$$

$$G_R = \frac{5(C_{11} - C_{12})C_{44}}{3(C_{11} - C_{12}) + 4C_{44}} \tag{6}$$

The anisotropy factor (A) is given as follows:

$$A = \frac{2C_{44}}{(C_{11} - C_{12})} \tag{7}$$

As the value of A becomes closer to unity (1), the material becomes isotropic. For an isotropic material, Young's modulus can be calculated by using bulk modulus (B) and shear modules (G) as follows:

$$E = \frac{9BG}{3B + G} \tag{8}$$

In addition, the Poisson's ratio can be computed by using Young's and bulk modulus as follows:

$$\sigma = \frac{1}{3}\left(1 - \frac{E}{3B}\right) \tag{9}$$

The thermodynamic properties including Debye temperature, heat capacity C_v, thermal expansion coefficient, and Grüneisen parameter are calculated in the quasi harmonic approximation using Gibbs2 code described in [31]. Helmholtz free energy is given as follows:

$$U = nk_BT\left[\frac{9}{8}\frac{\theta_D}{T} + 3\ln\left(1 - e^{-\frac{\theta_D}{T}}\right) - D\left(\frac{\theta_D}{T}\right)\right] \quad (10)$$

where the $D\left(\frac{\theta_D}{T}\right)$ function is given by

$$D\left(\frac{\theta_D}{T}\right) = 3\left(\frac{T}{\theta_D}\right)^3 \int_0^{\frac{\theta_D}{T}} \frac{x^3}{e^x - 1}dx \quad (11)$$

3 Results

3.1 Structural and Elastic Properties

The crystal structures of Au_2TiAl, Ru_2TiAl, and Zr_2TiAl alloys are shown in Figure 1. The total energy for different volumes around the equilibrium volume is calculated for the $L2_1$ phase. The calculated total energy is then fitted to Murnaghan's equation of state [32] in order to obtain their equilibrium lattice constants, the bulk modulus B, and its pressure derivative B'. The optimised lattice constant (a), bulk modulus (B), its pressure derivative B', elastic constants (C_{ij}), and Cauchy pressures (C_{12}–C_{44}) for Au_2TiAl, Ru_2TiAl, and Zr_2TiAl alloys are presented in Table 1. The lattice constants of all alloys are in a good agreement with theoretical and experimental values [16, 17, 21, 22]. The deviations of the computed lattice constant values of Au_2TiAl and Zr_2Tial alloys are about 1.14% and 0.16% from the experimental values [16, 20], which indicates that a satisfactory level of precision can be achieved in the density functional theory calculations. The computed bulk modulus of Zr_2TiAl is only ~2.93%, inconsistent with the calculated result of [22].

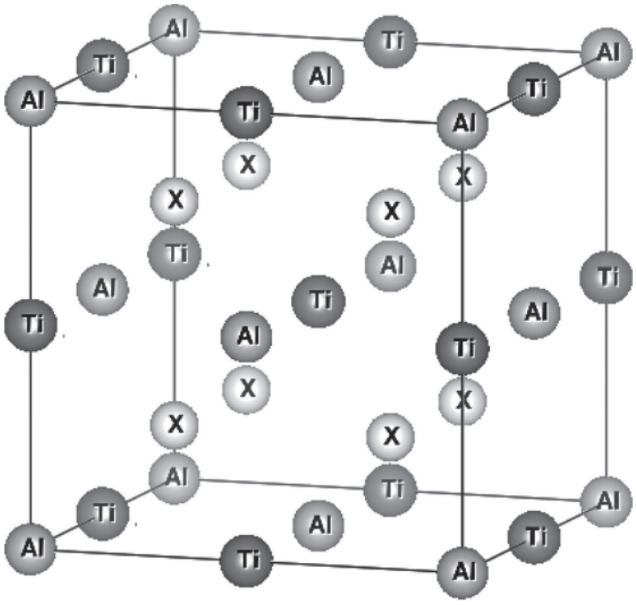

Figure 1: The crystal structure of the full-Heusler X_2TiAl (X = Au, Ru, and Zr) alloys.

Elastic constants are known as numbers that quantitatively reflect the elastic or non-elastic response of the material when a stress is applied on it. The elastic properties of a cubic crystal are generally characterised by three independent constants, namely, C_{11}, C_{12}, and C_{44}. The obtained values of C_{11}, C_{12}, and C_{44} for three alloys are given in Table 1, along with the available data in literature. To the best of our knowledge, the experimental or theoretical elastic constants of Au_2TiAl and Ru_2TiAl alloys have not yet been presented in the literature. Therefore, the results of two alloys in the $L2_1$ phase may serve as a base for future investigations. The three elastic constants for Zr_2TiAl are found to be larger than that of the results of Reddy and Kanchana [22] by about 7.80%, 0.35%, and

Table 1: The calculated values of lattice constants, bulk modulus, its pressure derivative of bulk modulus, Cauchy pressures, and elastic constants of X_2TiAl (X = Au, Ru, and Zr) alloys.

Alloy	Reference	a	B	B'	C_{11}	C_{12}	C_{44}	C_{12}–C_{44}
Au_2TiAl	This work	6.473	129.6	4.93	151.467	138.170	74.543	63.627
	Exp. [16]	6.400						
	FLASTO [17]	6.346						
Ru_2TiAl	This work	6.088	217.7	5.23	341.667	158.427	93.052	65.375
	FLASTO [17]	6.010						
	VASP [38]	6.087						
Zr_2TiAl	This work	6.821	98.5	3.09	117.514	91.100	63.565	27.535
	FP-LAPW [22]	6.840	96.875	–	109.006	90.782	58.129	32.653
	Exp. [21]	6.820						

9.35%, respectively. The mechanical stability evolution of alloys is also carried out based on their elastic constants. The necessity of mechanical stability in a cubic crystal makes the following constraints on the elastic constants [33]:

$$(C_{11} + 2C_{12}) > 0,\ C_{44} > 0,\ C_{11} > 0,\ \text{and}\ C_{11} - C_{12} > 0 \tag{12}$$

Table 1 exhibits that all alloys fulfil the stability condition of (12), including the fact that the values of C_{11} is higher than that of C_{12}. Equation (12) also leads to a restriction that the equilibrium bulk modulus should have a value between C_{11} and C_{12} ($C_{11} < B > C_{12}$), which is confirmed for all three alloys. Thus, it can be concluded that X_2TiAl alloys are stable in the $L2_1$ phase. The value of C_{11} also provides information about compressive resistance along the x-axis [32]. The value of C_{11} of Zr_2TiAl is lower than that of Au_2TiAl and Ru_2TiAl, indicating that Zr_2TiAl is more compressible along the x-axis than the other alloys. Cauchy pressures of three alloys, which describe the nature of bonding at the atomic level in metals and compounds, are calculated from the elastic constants. If Cauchy pressure has a value of more negative, the bonding is directional with angular character and shows a characteristic of a covalent material [34, 35]. In the opposite case (positive), the bonding is more metallic and nondirectional [36, 37]. Table 1 indicates that Cauchy pressures of alloys are positive, suggesting a metallic bonding for all alloys.

For further analysis of the mechanical properties of X_2TiAl alloys, the brittleness and ductility properties are also investigated via the bulk modulus to shear modulus (B/G) ratio and the Poisson ratio (σ), which are obtained by using C_{ij}. In general, the bulk modulus of a solid represents the resistance to a volume change and a measure of the average bond strength of atoms, whereas shear modulus represents the resistance to plastic deformation. According to Pugh's [35] criteria, X_2TiAl alloys are ductile because the B/G values of the three alloys are bigger than 1.75 as shown in Table 2. It can be also noticed that the Poisson's ratios of the three alloys are around 0.33; hence, all alloys have a ductile nature. The conclusions of both B/G and Poisson's ratio support each other. Additionally, the Poisson's ratio is used to estimate the bonding properties within the material and measure the stability of crystal against shear. As the Poisson's ratio increases, the plasticity of the crystal becomes better. The Poisson ratio is suggested as 0.1 for covalent materials and 0.25 for ionic materials in the literature [38]. The Poisson's ratios for Au_2TiAl, Zr_2TiAl, and Ru_2TiAl alloys are found to be 0.39, 0.34, and 0.31, respectively, which implies that the alloys have ionic-metal interaction. These results are in well accordance with Cauchy pressures of alloys mentioned previously. The total magnetic moment calculations indicate that Zr_2TiAl has a total magnetic moment of 2.02 μ_B per formula unit. This is in well accordance with the results of Reddy and Kanchana [22]. However, Au_2TiAl and Ru_2TiAl alloys do not show any magnetic moment; thus, these alloys are nonmagnetic materials.

The Young's modulus (E) of a material, which is a ratio of tensile stress to tensile strain, defines the stiffness and tensile elasticity of a material. From the calculations, Young's modulus of Au_2TiAl is 86.774 GPa, which is smaller than that of Zr_2TiAl (92.326 GPa) and Ru_2TiAl (243.266 GPa). As the value of E increases, the material becomes stiffer. It can be seen from Table 2 that Ru_2TiAl has the largest Young's modulus value among the three alloys; hence, Ru_2TiAl is the stiffest alloy among them. The anisotropy factor A is obtained as a measure of the degree of the elastic anisotropy of the crystals and presented in Table 2. For a complete isotropic material, the anisotropy factor value is 1. Deviation from this value defines the elastic anisotropy degree. As Table 2 illustrates, the calculated anisotropy factors of all alloys are higher than unity, showing that the studies alloys are elastically anisotropic. However, Ru_2TiAl's anisotropy factor is very close to unity.

According to Table 2, Au_2TiAl and Zr_2TiAl possess anisotropy; thus, two-dimensional directional dependence of Young's modulus has been computed for all alloys using EIAM code [39] and presented in Figure 2. It is known that for an isotropic material, the shape is spherical. Deviation from this shape indicates degree of anisotropy [40, 41]. It is clear from Figure 2 that Ru_2TiAl is isotropic at all planes, whereas Au_2TiAl and Zr_2TiAl are anisotropic.

Table 2: The computed shear modulus G (GPa), B/G ratio, anisotropy factor A, Young's modulus E (GPa), Poisson's ratio, and total magnetic moment of X_2TiAl (X = Au, Ru, and Zr) alloys.

Alloy	Reference	B	G	B/G	A	E	σ	μ_B
Au_2TiAl	This work	142.603	31.022	4.596	11.212	86.774	0.39	0
Ru_2TiAl	This work	219.507	92.476	2.373	1.015	243.266	0.31	0
Zr_2TiAl	This work	99.905	34.297	2.912	4.81	92.326	0.34	2.02

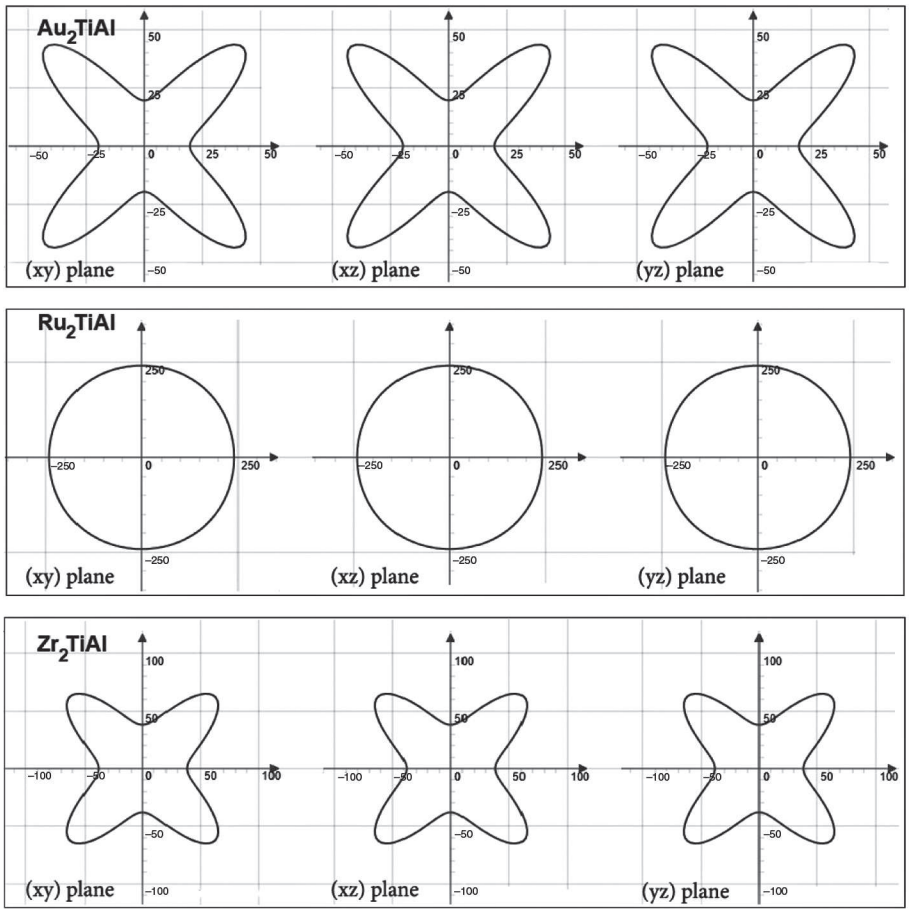

Figure 2: Two-dimensional directional dependence of the Young's modulus of X_2TiAl (X = Au, Ru, and Zr) alloys.

3.2 Electronic and Phonon Properties

The electronic band structures of X_2TiAl alloys are presented in Figure 3, along the high-symmetry directions in the Brillouin zone.

Figure 3 illustrates that the band lines and finite DOS cut the Fermi energy level for all alloys; therefore, these alloys have a metallic character. It is shown that there is no gap at the Fermi level, and total density of states are 1.329 and 2.25 states eV^{-1} cell for Au_2TiAl and Ru_2TiAl, respectively. The bands that cross the Fermi level can be seen in both majority and minority spin states determining the metallic nature of Zr_2TiAl alloy (see Fig. 4).

The band states for these alloys are determined by calculating the total and partial densities of states. The main characters of the computed results for the three alloys are in well accordance with the previous reported studies of electronic structure [22, 42]. There are peaks above and below the Fermi level from the total and partial densities of Au_2TiAl and Ru_2TiAl, as shown in Figure 4. The main contributions to the bands below the Fermi level are due to Au 5d states for Au_2TiAl and Ru 4d states for Ru_2TiAl, whereas above the Fermi level, they are mainly due to Ti 3s states for both alloys. For Zr_2TiAl, it is seen that the majority and minority spin contributions of the DOS in the Fermi level are due to the '*d*' electrons of the Zr and Ti atoms.

The phonon dispersion curves along the Γ-K-Γ-W-L directions in the first Brillouin zone are computed for X_2TiAl alloys and shown in Figure 5. There are no imaginary phonon frequencies in the whole Brillouin zone for X_2TiAl alloys. This suggests that three alloys are dynamically stable in the $L2_1$ phase. As X_2TiAl alloys have four atoms in their unit cell, the phonon spectrum should have 12 branches; three of them is being acoustic (lowest three) and nine of them is being optical. The frequencies of the optical phonon modes of X_2TiAl at the zone centre are calculated as 2.567, 5.750, and 6.754 THz for Au_2TiAl; 5.812, 6.395, and 9.876 THz for Ru_2TiAl; and 3.312, 4.625, and 7.723 THz for Zr_2TiAl. It can be seen that the optical phonons of Au_2TiAl overlap and fall in the frequency region between 4.74 and 7.6 THz. On the other hand, for Ru_2TiAl and Zr_2TiAl alloys, optical phonon frequencies are separated. Examination of the atomic masses of Au, Ru, Zr, Ti, and Al allows us to understand this difference between

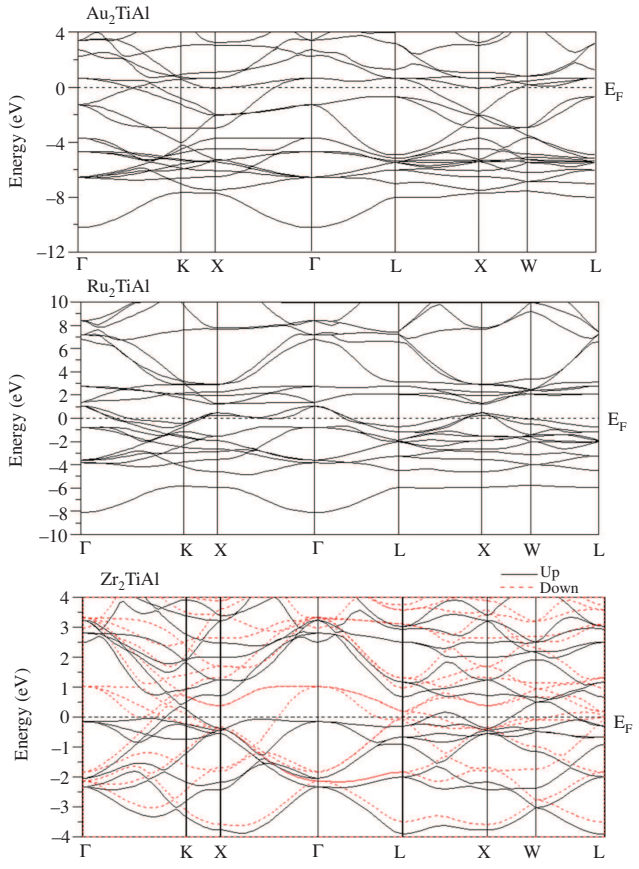

Figure 3: The electronic band structure of X_2TiAl (X = Au, Ru, and Zr) alloys.

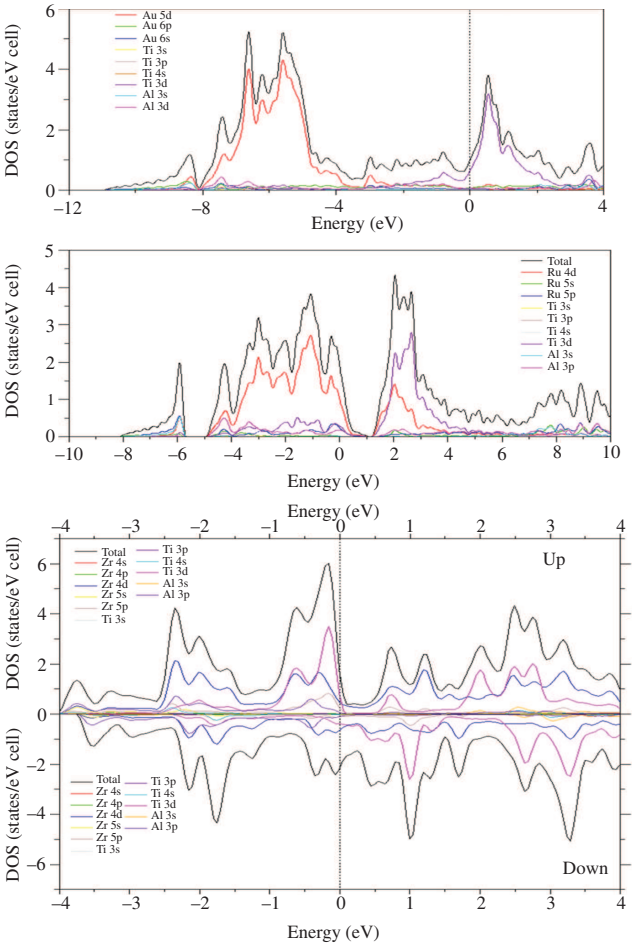

Figure 4: The total and partial densities of states of X_2TiAl (X = Au, Ru, and Zr) alloys.

the alloys. The phonon partial density of states of alloys shows that the upper optical frequency is due to the lighter Al atoms, whereas the lower frequency region is due to the heavier Au (Ru and Zr) atoms. Ti atoms vibrate in the middle phonon frequency region for all alloys.

3.3 Thermodynamic Properties

The thermodynamic properties are obtained within the quasi-harmonic approximation for different temperatures from the energy-volume relation. One of the important thermodynamic property for a solid is the Debye temperature, which provides information about many other quantities such as specific heat, melting temperature, and elastic stiffness. It is also related to the maximum thermal vibration frequency of a solid. Figure 6 demonstrates the dependence of the Debye temperature on temperature. As can be seen from the figure, the Debye temperature decreases slowly over the temperature range of 0–1500 K for all alloys. This variation in Debye temperature with temperature indicates that the thermal vibration frequency of the particles changes with temperature. The slow variation reflects the small effect of temperature on Debye temperature. In addition, vibrational frequency is proportional to the square root of the stiffness within the harmonic approximation; the 'stiffness' of solids can also be estimated from Debye temperature and called as 'Debye stiffness' [43]. Based on that, it can be said that Debye stiffness of Ru_2TiAl is higher than that of the Au_2TiAL and Zr_2TiAl alloys.

The vibrational contributions due to temperature change to the specific heat capacities of X_2TiAl alloys at a constant volume (C_V) is estimated using ab initio calculation with the quasi-harmonic approximation, too. The results are presented in Figure 7. A rapid increase is observed up to 200 K, and then saturation is reached, which is called Dulong-Petit limit as seen in the figure. The values of specific heat capacities are close to those reported by Dulong-Petit [44] at high temperatures. However, below 200 K, heat capacity is strongly dependent on the temperature. The heat capacity reaches to zero

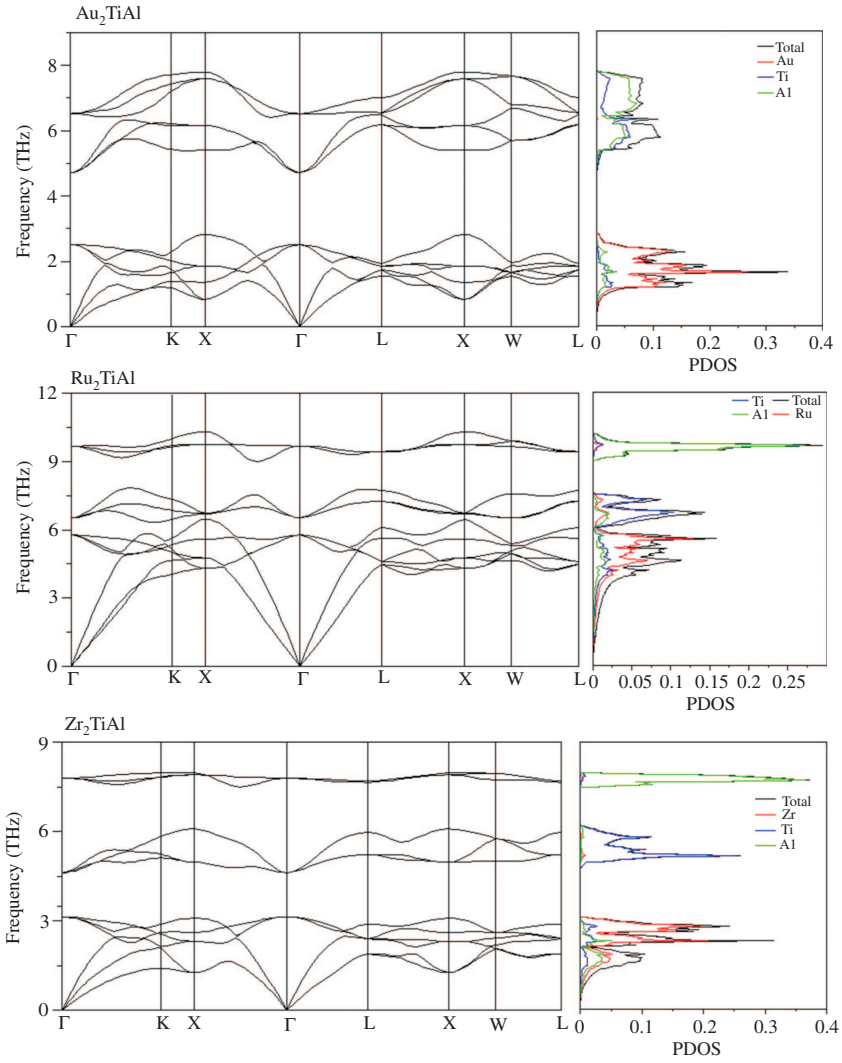

Figure 5: Full phonon dispersion spectra and their total and projected densities of states of X_2TiAl (X = Au, Ru, and Zr) alloys.

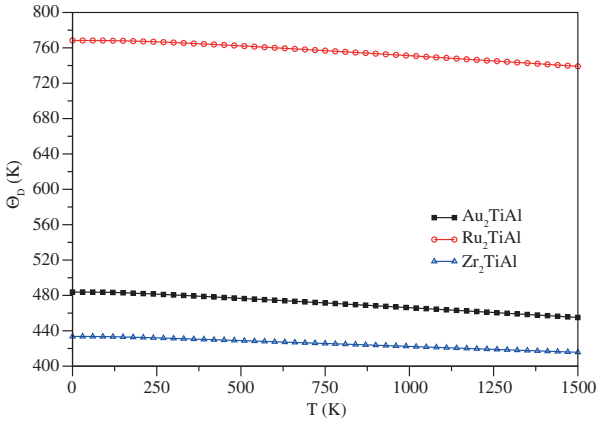

Figure 6: Variations in the Debye temperature for X_2TiAl (X = Au, Ru, and Zr) alloys.

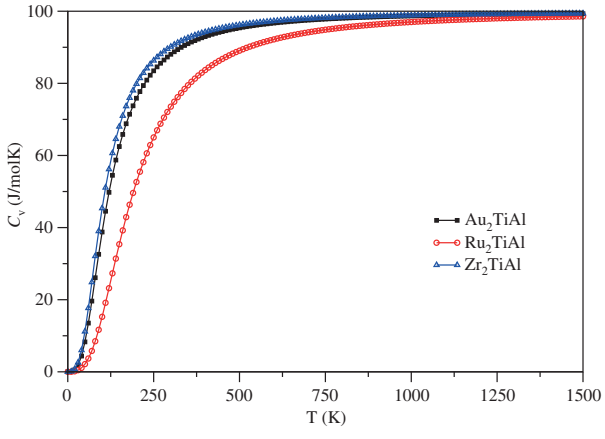

Figure 7: The temperature dependence of the specific heat capacities at constant volume (C_V) of X_2TiAl (X = Au, Ru and Zr) alloys.

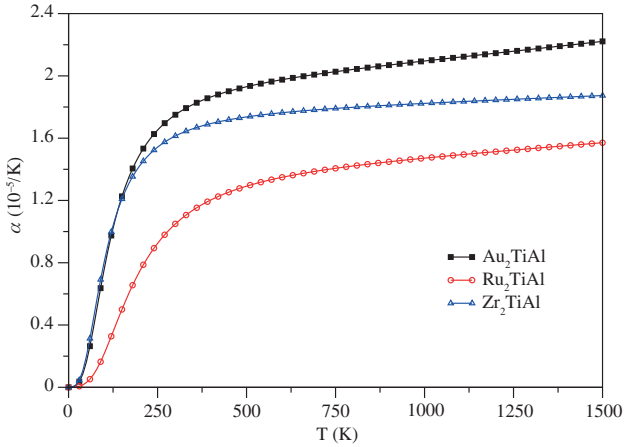

Figure 8: Variations of thermal expansion coefficient with temperature for X_2TiAl (X = Au, Ru, and Zr) alloys.

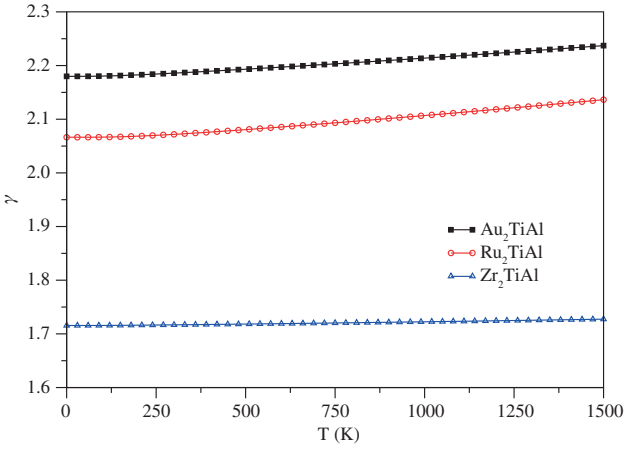

Figure 9: Grüneisen parameter versus temperature for X_2TiAl (X = Au, Ru, and Zr) alloys.

quickly as the temperature reaches to absolute zero. Unfortunately, there is no experimental data in the literature to compare these findings for these alloys to the best of our knowledge.

The variations in volume thermal expansion coefficients of all the three alloys versus temperature are shown in Figure 8. As it is clearly seen from the figure, thermal coefficients of all alloys rapidly increase up to 300 K. After this point, it increases gradually and becomes flat. Another important parameter that is obtained from the quasi-harmonic approximation is the Grüneisen parameter, which describes the anharmonic effects in the vibrating lattice and can be used to estimate the anharmonic properties of a solid. Grüneisen parameters of all alloys are presented in Figure 9. It seems that Grüneisen parameters seem to stay flat and show little sensitivity to temperature. One can notice that the Grüneisen parameter is not zero at 0 K, suggesting that thermal expansion coefficient and heat capacity approach zero in the same asymptotic way. In fact, the Grüneisen parameter at 0 K is proportional to the logarithmic derivative of T^3 coefficient in the heat capacity with respect to volume [45].

4 Conclusion

In this study, we have performed pseudopotential calculations to investigate stabilities, mechanical, electronic, thermodynamic, and magnetic properties of X_2TiAl (X = Au, Ru, and Zr) alloys. The obtained values of lattice constants of alloys are found to be in good agreement with the existing experimental and theoretical data. The computed elastic constants illustrated that all three alloys are mechanically stable. Electronic band structures and their total and partial densities of states for all the three alloys are in line with the existing data. The band structure diagrams confirm the metallicity of alloys in the $L2_1$ phase. Full phonon dispersion spectra and their total and projected densities of states for alloys in the $L2_1$ phase have been calculated for the first time in the framework of density functional perturbation theory. Several thermodynamic properties such as the specific heat capacities, thermal expansion coefficient, and Debye temperatures of alloys are obtained within the quasi harmonic approximation using the Gibbs2 code.

References

[1] F. Heusler, Verhandlungen der Deutschen Physikalischen Gesellschaft **5** (1903).
[2] R. A. de Groot, F. M. Mueller, P. G. van Engen, and K. H. J. Buschow, Phys. Rev. Lett. **50**, 2024 (1983).
[3] C. K. Hem, H. F. Gerhard, and F. Claudia, J. Phys. D: Appl. Phys. **40**, 6 (2007).
[4] S. Galehgirian and F. Ahmadian, Solid State Commun. **202**, 52 (2015).
[5] F. Lei, C. Tang, S. Wang, and W. He, J. Alloys Compd. **509**, 17 (2011).
[6] J. Toboła and J. Pierre, J. Alloys Compd. **296**, 1 (2000).
[7] S. Bhattacharya, A. L. Pope, R. T. Littleton IV, T. M. Tritt, V. Ponnambalam, et al., Appl. Phys. Lett. **77**, 16 (2000).
[8] M. Wuttig, J. Li, and C. Craciunescu, Scripta Mater. **44**, 10 (2001).
[9] Y. Sutou, Y. Imano, N. Koeda, T. Omori, R. Kainuma, et al., Appl. Phys. Lett. **85**, 19 (2004).
[10] K. Gofryk, D. Kaczorowski, and A. Czopnik, Solid State Commun. **133**, 10 (2005).
[11] H. Nakamura, Y. Kitaoka, K. Asayama, Y. Onuki, and T. Komatsubara, J. Magn. Magn. Mater. **76–77**, 467 (1988).
[12] S. Takayanagi, S. B. Woods, N. Wada, T. Wataneke, Y. Onuki, et al., J. Magn. Magn. Mater. **76** (1988).

[13] K. Gofryk, D. Kaczorowski, T. Plackowski, A. Leithe-Jasper, and Yu. Grin, Phys.Rev. B **72**, 9 (2005).
[14] D. Kaczorowski, K. Gofryk, T. Plackowski, A. Leithe-Jasper, and Yu. Grin, J. Magn. Magn. Mater. **290**, (2005).
[15] B. Akgenc, A. Kinaci, C. Tasseven, and T. Cagin, Mater. Chem. Phys. **205**, 315 (2018).
[16] R. Marazza, R. Ferro, and G. Rambaldi, J. Less Common Met. **39**, 2 (1975).
[17] R. E. Watson, M. Weinert., and M. Alatalo, Phys. Rev. B **57**, 19 (1998).
[18] M. Yin and P. Nash, J. Alloys Compd. **634**, 70 (2015).
[19] F. Yang, et al., J. Alloys Compd. **585**, 325 (2014).
[20] D. Sornadurai, V.S. Sastry, V. Thomas Paul, R. Flemming, F. Jose, et al., Intermetallics **24**, 1267 (2012).
[21] D. Sornadurai, R.L. Flemming, and V.S. Sastry, AIP Conf. Proc. **1349**, 1 (2011).
[22] P. V. S. Reddy and V. Kanchana, AIP Conf. Proc. **1591**, 1 (2014).
[23] P. Hohenberg and W. Kohn, Phys. Rev. **136**, 3B (1964).
[24] W. Kohn and L. J. Sham, Phys. Rev. **140**, 4A (1965).
[25] G. Paolo, et al., J. Phys.: Condens. Matter **21**, 39 (2009).
[26] J. P. Perdew, K. Burke, and M. Ernzerhof, Phys. Rev. Lett. **77**, 18 (1996).
[27] M. Methfessel and A. T. Paxton, Phys. Rev. B **40**, 6 (1989).
[28] S. Baroni, P. Giannozzi, and A. Testa, Phys. Rev. Lett. **58**, 18 (1987).
[29] S. Baroni, S. de Gironcoli, A. Dal Corso, and P. Giannozzi, Rev. Mod. Phys. **73**, 2 (2001).
[30] S. Baroni, P. Giannozzi, and E. Isaev, Rev. Mineral. Geochem. **71**, 1 (2010).
[31] R. Singh, J. Mag. Alloys **2**, 4 (2014).
[32] F. D. Murnaghan, Proc. Natl. Acad. Sci. USA. **30**, 9 (1944).
[33] N. Arıkan, A. İyigör, A. Candan, M. Özduran, A. Karakoç, et al., J. Mat. S. **49**, 12 (2014).
[34] R. Johnson, Phys. Rev. B **37**, 8 (1988).
[35] S. F. Pugh, Phil. Mag. J. Sci. **45**, 367 (1954).
[36] D. G. Pettifor, Mater. Sci. Technol. **8**, 4 (1992).
[37] C. Çoban, Z. Naturforsch A **72**, 9 (2017).
[38] V. V. Bannikov, I. R. Shein, and A. L. Ivanovskii, Phys. Status Solidi-R **1**, 3 (2007).
[39] A. Marmier, Z. A. D. Lethbridge, R. I. Walton, C. W. Smith, S. C. Parker, et al., Comput. Phys. Commun. **181**, 12 (2010).
[40] G. Surucu, C. Kaderoglu, E. Deligoz, and H. Ozisik, Mater. Chem. Phys. **189**, 90 (2017).
[41] G. Surucu, Mater. Chem. Phys. **203**, 106 (2018).
[42] M. Gilleßen, Made-to-Measure Products and Substitute for Analytics: About the Quantum-Chemical Studies of Some Ternary Intermetallic Phases, Oxford, Germany, 2010.
[43] T. Tohei, A. Kuwabara, F. Oba, and I. Tanaka, Phys. Rev. B **73**, 6 (2006).
[44] A. T. Petit, Ann. Chim. Phys. **10**, 395 (1819).
[45] S. Wei, C. Li, and M. Y. Chou, Phys. Rev. B **50**, 19 (1994).